Title	Reconstruction of sea ice concentration in northern Baffin Bay using deuterium excess in a coastal ice core from the northwestern Greenland Ice Sheet
Authors	Yutaka Kurosaki, Sumito Matoba, Yoshinori Iizuka, Masashi Niwano, Tomonori Tanikawa, Takuto Ando, Akira Hori, Atsushi Miyamoto, Shuji Fujita, Teruo Aoki
Citation	Journal of Geophysical Research: Atmospheres, 125(16), 1-19, 2020
Issue Date	2020-8-18
Type	Journal Article
URL	https://doi.org/10.1029/2019JD031668
Right	
Textversion	publisher

JGR Atmospheres

Key Points:
- The moisture source for precipitation at the ice core drilling site on the northwestern Greenland Ice Sheet is the northern Baffin Bay
- Spring deuterium excesses in the ice core negatively correlated with sea ice concentrations in the northern Baffin Bay from 1979–2005
- The reconstructed sea ice concentrations were low for the early twentieth century and varied with atmospheric and oceanographic factors

Supporting Information:
- Supporting Information S1

Correspondence to:
Y. Kurosaki and S. Matoba,
kurosaki_yutaka@frontier.hokudai.ac.jp;
matoba@pop.lowtem.hokudai.ac.jp

Reconstruction of Sea Ice Concentration in Northern Baffin Bay Using Deuterium Excess in a Coastal Ice Core From the Northwestern Greenland Ice Sheet

Yutaka Kurosaki[1,2] [ID], Sumito Matoba[2] [ID], Yoshinori Iizuka[2] [ID], Masashi Niwano[3] [ID], Tomonori Tanikawa[3] [ID], Takuto Ando[4] [ID], Akira Hori[5] [ID], Atsushi Miyamoto[6], Shuji Fujita[7] [ID], and Teruo Aoki[3,7] [ID]

[1]Graduate School of Environmental Science, Hokkaido University, Sapporo, Japan, [2]Institute of Low Temperature Science, Hokkaido University, Sapporo, Japan, [3]Meteorological Research Institute, Japan Meteorological Agency, Tsukuba, Japan, [4]Arctic Research Center, Hokkaido University, Sapporo, Japan, [5]Kitami Institute of Technology, Kitami, Japan, [6]Institute for the Advancement of Higher Education, Hokkaido University, Sapporo, Japan, [7]National Institute of Polar Research, Tokyo, Japan

Abstract Variations in the conditions of sea ice in the northern part of Baffin Bay and North Open Water polynya influence human activity in northwestern Greenland through oceanic circulation and heat balance between air and sea. To evaluate the impact of variations in sea ice conditions on the surrounding environment, it is important to understand the mechanism of sea ice variations over long periods. In this study, we estimated the age of the SIGMA-A ice core collected northwestern Greenland Ice Sheet and researched the relationship between annual or seasonal deuterium excess (d-excess) and seasonal sea ice concentration. We found that a temporal variation in the spring d-excess in the ice core negatively correlated significantly with that of sea ice concentration in February–April in northern Baffin Bay from 1979–2005 ($r = -0.61$, $p < 0.001$). Using this relationship, we reconstructed the temporal variations in sea ice concentrations for 100 years from the ice core drilled in the northwestern Greenland Ice Sheet. The sea ice concentration in the early twentieth century was lower than that in the present. The decrease in sea ice concentration was consistent with analytical results for marine sediments obtained from Baffin Bay. We also suggested that the sea ice concentration was controlled by atmospheric conditions from the 1920s to 1940s based on examinations of correlations with the North Atlantic Oscillation index and air temperature in Ilulissat and by oceanographic conditions from 1945–1955, 1959–1969, and 1982–1992 based on the Atlantic Multidecadal Oscillation index and meridional heat transport to western Greenland.

1. Introduction

Baffin Bay is located between Greenland in the east and Baffin Island, Devon Island, and Ellesmere Island in the west. Baffin Bay is today covered with seasonal sea ice from winter to spring. In northwestern Greenland, facing Baffin Bay, there are several villages whose people hunt and fish on sea ice and move between the villages on sea ice by dog sledge and skidoos during winter and spring. Therefore, recent changes in sea ice conditions influence human activities in this region. The frequency of winter breakup of sea ice in front of Siorapaluk village, which is the northernmost village in this region, has increased remarkably since the 2000s (Matoba & Yamasaki, 2018).

The North Open Water (NOW) polynya extends from 76 to 79°N and 70 to 80°W between northwestern Greenland and Ellesmere Island. The NOW polynya is categorized as a latent heat polynya (Melling et al., 2001). When sea ice forms by wind and ocean current actions, new ice is advected away by winds and currents (Dumont et al., 2009), and latent heat is released from the ocean surface (Minnett & Key, 2007). The polynya is also a water vapor source for precipitation surrounding the polynya (Minnett & Key, 2007). Thus, the formation of a polynya influences the heat balance between air and sea, oceanic circulation, and meteorological conditions surrounding the polynya.

An ice core is a useful tool to reconstruct climate and environmental variations in the past or recent past in polar areas where meteorological data recorded continuously are few. Among the many signals detected in
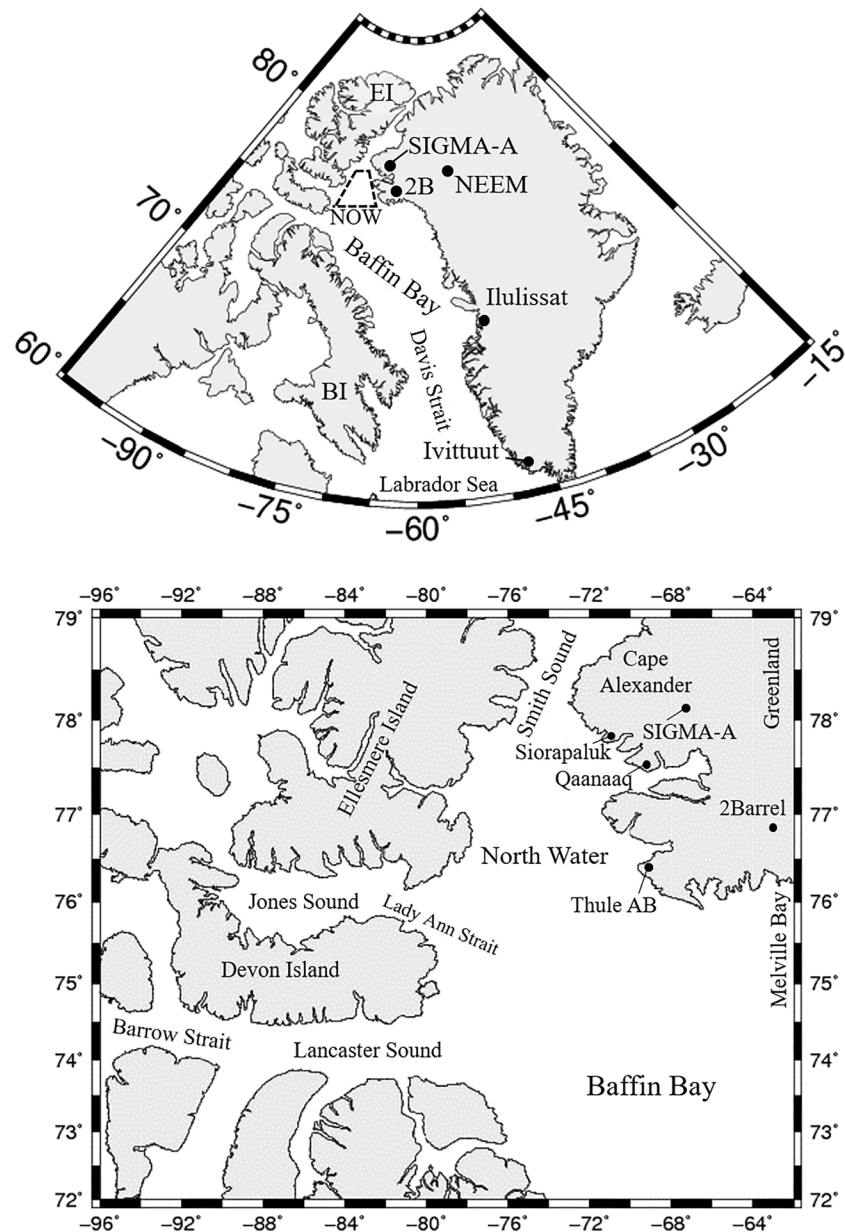
Figure 1. Maps around Greenland (upper panel) (Kurosaki et al., 2018) and north open water (lower panel). The SIGMA-A site is located on the northwestern coast of the Greenland Ice Sheet. EI = Ellesmere Island; 2B = 2Barrel; Thule AB = Thule Air Base.

ice cores, water stable isotopes (δD and $\delta^{18}O$) are important signals for reconstructing air temperatures and precipitation amounts. There is a correlation between δD and $\delta^{18}O$ of water (Craig, 1961), and Dansgaard (1964) defined as the deuterium excess (d-excess) by the following equation 1:

$$d - excess = \delta D - 8 \, \delta^{18}O. \tag{1}$$

The d-excess reflects ocean surface conditions in water vapor source regions for precipitation and does not change during transport of an air mass with any condensation processes (Merlivat & Jouzel, 1979). Therefore, the d-excess is recognized as a tracer indicating environmental conditions at the moisture source, such as sea surface temperature (SST), air temperature, wind speed, and relative humidity (Gat, 1996;

Uemura et al., 2008). Recently, relationships between d-excess in water vapor or precipitation and sea ice conditions in water vapor source regions have been reported as below. In polar regions, d-excess in water vapor becomes high over open water areas surrounded by sea ice (Kurosaki et al., 2018; Steen-Larsen et al., 2014). When cold air blows down to an open water area, strong evaporation occurs due to a steep temperature gradient between the sea surface and air above the sea surface, and strong evaporation results in high d-excess in water vapor (Kurita, 2011; Kurosaki et al., 2018). Based on the relationship between sea ice conditions and d-excess in water vapor, temporal variations in sea ice conditions have been reconstructed from ice core analyses. Sinclair et al. (2014) reconstructed temporal variations in sea ice in the Ross Sea, Antarctica, for 130 years using a negative correlation between d-excess in a coastal ice core obtained in Antarctica and sea ice area in the Ross Sea ($r = -0.53$, $p < 0.01$). On the other hand, Osterberg et al. (2015) showed a positive correlation with the annual mean of d-excess in an ice core from the northwestern Greenland Ice Sheet ($r = 0.61$, $p < 0.01$). Thus, a certain relationship between d-excess in ice core and sea ice conditions is suggested. However, that relationship differs depending on the position of an ice core drilling site and moisture source for precipitation at the ice core drilling site.

In this paper, we elucidate a relationship between d-excess in an ice core obtained from the coastal area of northwestern Greenland and sea ice concentration in Baffin Bay and NOW, reconstruct the temporal variations in sea ice concentration for 100 years, and discuss the mechanism of the temporal variations in sea ice concentration.

2. Materials and Methods

2.1. SIGMA-A Ice Core

The SIGMA-A observation site (78°03′06″N, 67°37′42″W, 1,490 m above sea level (a.s.l.)) is located 70 km northeast of the town of Qaanaaq in northwestern Greenland and lies on the ridge of the Hayes Peninsula, which is north of Qaanaaq (Figure 1) (Aoki et al., 2014). Because the elevation of the drilling site is relatively low and the distance from the coastline is remarkably short, reconstructed information from the ice core can reflect the nearby land and ocean. Matoba et al. (2014) conducted several snow pit observations and chemical analyses of the snow along the ridge and suggested that the fluctuations in water isotopes and chemical substances in the snow resulted from water vapor and air transport from the south generated by an atmospheric depression developed over Baffin Bay. Therefore, profiles of water isotopes and chemical substances in the ice core from the SIGMA-A site can reflect the variations in sea ice conditions in Baffin Bay. According to previous research at the SIGMA-A site, the annual average surface mass balance was 0.27 m water equivalent per year (w. eq. year^{-1}) between 1975 and 2010 (Matoba et al., 2016; Yamaguchi et al., 2014). From May to June 2017, we drilled a 60.06 m-deep ice core (Matoba et al., 2018). We used an electromechanical ice-core drilling system developed by the Institute of Low Temperature Science (ILTS), Hokkaido University (HU) (Shiraiwa et al., 2004). The ice core samples were placed in polyethylene bags and packed into insulated boxes without any cutting processes, and they were then kept frozen at approximately −25°C during shipment to the ILTS-HU in Japan. Ice core sections were preserved at −50°C in the cold laboratory of the institute until chemical analysis.

2.2. Ice Core Analysis

All chemical analyses of the ice core were conducted at the ILTS-HU. The core samples were prepared for analysis of the stable isotopes of water in a cold laboratory (−20°C). Ice core samples with a thickness of 90 mm were cut longitudinally into three parts (thicknesses of 5, 75, and 10 mm) with a band saw (supporting information Figure S1). One of the 5 mm-thick sections was horizontally cut at 25 mm intervals for analysis of the stable isotopes of water. The subsamples were placed into clean polyethylene bags, melted at ambient temperature, and decanted into glass bottles with an inner cap. The stable oxygen and hydrogen isotope compositions of water were measured using a water stable isotope analyzer (L2130-I, Piccaro Inc.) with an evaporating device (A0212, Picarro Inc.). The analytical precisions of $\delta^{18}O$ and δD were 0.08‰ and 0.8‰, respectively.

Using the residue after measurements of the stable isotopes of water, tritium concentrations were measured using a liquid scintillation counter (LSC-LB3, Aloka Co., Ltd.) to identify the reference horizon of the H-bomb test in 1963. The spatial resolution of the measurement of tritium content was 48 mm.

To identify volcanic signals as reference horizons for ice core chronology, the continuous electrical conductivity was measured using a dielectric profiling system (DEP). DEP has been developed to study the solid electrical conductivity of ice cores (e.g., Moore & Paren, 1987; Wilhelms et al., 1998). In this study, we used a system developed by the National Institute of Polar Research, Japan (e.g., Fujita et al., 2016; Iizuka et al., 2017). We measured electrical conductivity at 250 kHz under a temperature of −22°C with a spatial resolution of 20 mm. Then, to obtain the accumulation rate of the ice core, a continuous density profile of the ice core was obtained using an X-ray transmission method (Hori et al., 1999). The intensity of X-rays transmitted through an ice core sample was continuously measured using an X-ray detector during translation of the sample across the beam. The X-ray intensity profile was then converted to a density profile using a calibration curve for X-ray absorption based on ice thickness. The spatial resolution of the density profile was approximately 1 mm. We used the 75 mm-thick section of the ice core.

The concentration of Cl^-, SO_4^{2-}, and Na^+ were measured by ion chromatography (Thermo Scientific, ICS-2100). We used Dionex CS12-A column with 20 mM methanesulfonic acid eluent and Dionex AS-17A column with 1–18 mM KOH gradient eluent for cations and anions, respectively. The analysis precision of the ion concentrations was 10%. Non-sea-salt (nss) SO_4^{2-} was calculated by the ratio of Na^+ and SO_4^{2-} ($SO_4^{2-}/Na^+ = 0.038$) (Wilson, 1975).

2.3. Moisture Source Diagnosis

To identify the source of moisture for precipitation at SIGMA-A, we used a part of the Lagrangian moisture source diagnostic (LMSD) technique introduced by Sodemann et al. (2008). The diagnostic method is based on analyzing the backward trajectory of an air mass. The change in the specific humidity within an air mass along its trajectory during a certain time interval is generally the net result of moisture uptake into the air mass due to evaporation and moisture scavenging from the air mass due to precipitation (James et al., 2004; Stohl & James, 2004). The difference of specific humidity within an air mass along its trajectory during 6-hr time interval is shown as below (Sodemann et al., 2008).

$$\Delta q(t) = q\left(\vec{x}(t)\right) - q\left(\vec{x}(t - 6h)\right). \tag{2}$$

$\vec{x}(t)$ is the air mass position at time t. In this study, $\vec{x}(t)$ was estimated by the 10-day backward trajectories at 00-, 06-, 12-, and 18-hr (UT) of precipitation days, which extracted from ERA-interim 6-hr time interval data set, at SIGMA-A calculated by the National Oceanographic and Atmospheric Administration (NOAA) hybrid single-particle Lagrangian integrated trajectory (HYSPLIT) model (Stein et al., 2015) with National Centers for Environmental Prediction (NCEP) reanalysis data set which grid interval was 2.5°. $q\left(\vec{x}(t)\right)$ was applied the specific humidity, which was extracted from ERA-interim 6-hr time interval and 0.75° horizontal interval data set, closest to the air mass position at time t. We integrated every moisture uptake into an air mass due to evaporation ($\Delta q(t) > 0$) using the Equation 2 and ignored the uptake of moisture during transport above 1,500 m a.s.l., land areas including the ice sheet and ocean areas where the sea ice concentration was more than 99% and the scavenging of moisture along the all trajectory. The starting points of trajectories were 500 m above ground level (a.g.l.) and 1,000 m a.g.l. at the SIGMA-A site, and the time interval was 6-hr. The specific humidity used in this analysis defined a vertical layer averaged at pressure levels from 850 to 1,000 hPa. We calculated integrated monthly values of moisture uptake under the above conditions from 1979 to 2016 at each grid of 1.0° horizontal interval.

2.4. Meteorological and Climatological Reanalysis Data

The SIGMA-A ice core could reconstruct environmental changes over the last 100 years around SIGMA-A site and Baffin Bay. Most instrumental or reanalysis data sets in these regions are not enough to compare with the ice core data over the last 100 years. Therefore, we used climate indices to elucidate the mechanism of climate changes reconstructed by the ice core data.

The North Atlantic Oscillation (NAO), which is a representative indicator of Northern Hemispheric climate variability, is based on the difference between the Icelandic low and the Azores high. In the positive NAO phase in winter, the gradient between the Icelandic low and Azores high is strong (Hurrell, 1995). Northerly wind becomes dominant, and surface temperature is lower across western Greenland when the
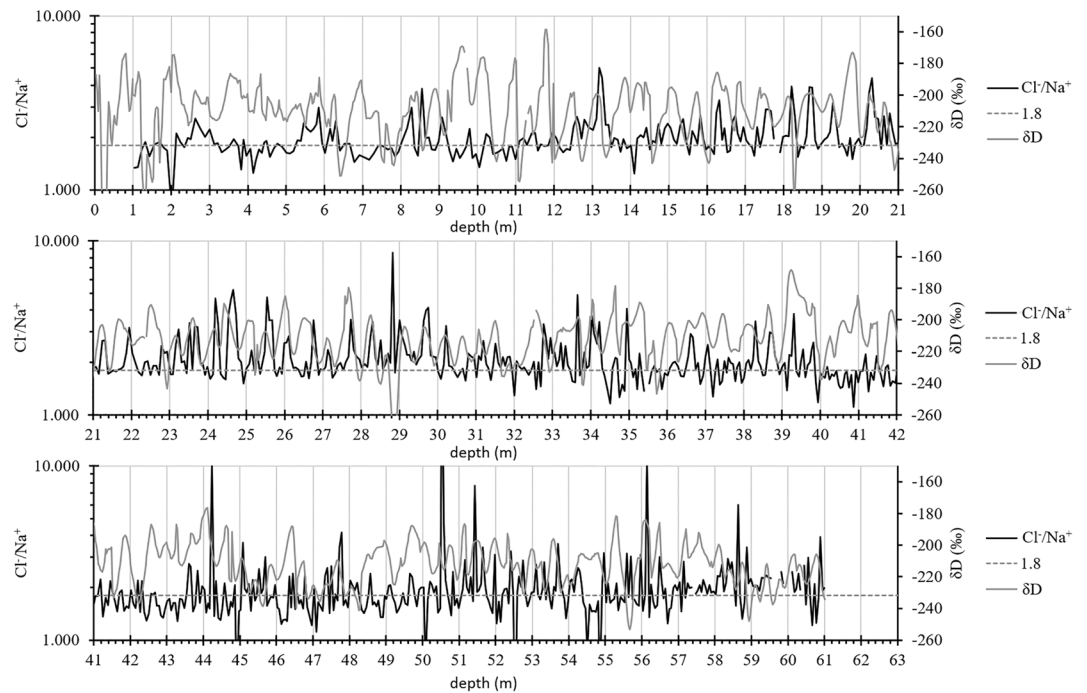
Figure 2. The vertical profile of Cl^-/Na^+ (black line) and δD (gray line) in SIGMA-A ice core. The gray dashed line is the weight ratio Cl^- to Na^+ in seawater (1.80).

Icelandic low is developed (Grumet et al., 2001). We used the monthly data set of the NAO index supplied by the Climatic Research Unit, University of East Anglia (Jones et al., 1997). The NAO index data were extended back to 1821 by instrumental pressure measurements from Gibraltar in southernmost Iberia and from southwestern Iceland (Jones et al., 1997).

The Atlantic Meridional Oscillation (AMO) is defined by the alternation of warm and cold SST anomalies in the North Atlantic Ocean (Kerr, 2000). We used the monthly data set of the AMO index supplied by the Earth System Research Laboratory (ESRL) (Enfield et al., 2001).

The surface oceanic circulation along the western coast of Greenland is dominated by the West Greenland Current (WGC), and the water mass is transported northward (Ribergaard et al., 2008). Warm water masses flow into the NOW from the southeastern region via the WGC (Melling et al., 2001). We estimated the heat flux of the warmer current as the vertically integrated heat transport (VIHT) supplied by the Ocean Analysis/Reanalysis System 3 (ORA-S3), ECMWF (Balmaseda et al., 2008). Moreover, we used the meridional component of VIHT and averaged between 60–61°N and 48–54°W.

The sea ice concentration, precipitation amount, and specific humidity used in this study were from the ERA-interim reanalysis data set supplied by the European Center for Medium-Range Weather Forecasts (ECMWF) (Dee et al., 2011).

3. Result and Discussion

3.1. Dating and Annual Accumulation Rate of the SIGMA-A Ice Core

Figure 2 shows vertical profiles of δD and Cl^-/Na^+. The δD profile exhibits regular cyclic variations. At several Greenland sites, $\delta^{18}O$ and δD have maximum values in summer and minimum values in winter (e.g., Kuramoto et al., 2011; Legrand & Mayewski, 1997; Oyabu et al., 2016). Thus, $\delta^{18}O$ and δD here have similar variations (Figure 3), and we recognize the regular cyclic variations in δD as a seasonal cycle. Cl^-/Na^+ also have positive peaks in summer at several site (e.g., Dibb et al., 2007; Furukawa et al., 2017). We recognize periodic peaks of Cl^-/Na^+ in the ice core as summer. Thus, we checked annual layers by counting negative peaks of δD and summer peaks of Cl^-/Na^+ (Figure 2, Table S1).
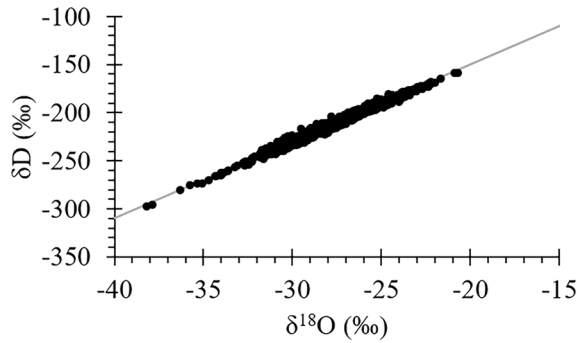
Figure 3. Relationship between δD and δ^{18}O in the SIGMA-A ice core (black circles). The gray line is the meteoric water line (δD = 8 × δ^{18}O + 10). δD is significantly correlated with δ^{18}O ($r = 0.99$, $p < 0.01$).

Figures 4 and 5 show vertical profiles of δD, nssSO$_4^{2-}$ concentration, tritium concentration, electrical conductivity, Cl$^-$/Na$^+$, ice layer thickness, and d-excess. We extracted significantly large (>2σ) peaks from vertical profiles of nssSO$_4^{2-}$ concentration, tritium concentration, electrical conductivity, and Cl$^-$/Na$^+$ except for ice layers where chemical species were relocated by melt water (Figure 6).

The age of the ice core was determined by identifying the reference horizons of the tritium peak originating from the H-bomb test and volcanic signals. A sharp tritium peak was found at 29.58–29.94 m, which is the reference horizon of H-bomb testing in 1963 (Clausen & Hammer, 1988) (Figure 4A).

It was difficult to find clear volcanic peaks from only nssSO$_4^{2-}$ during late twentieth century because anthropogenic SO$_x$ in atmosphere increased in this period. Therefore, we identified volcanic signals by electrical conductivity and Cl$^-$/Na$^+$ in addition to nssSO$_4^{2-}$ (Figures 4 and 5). There were continuous peaks of nssSO$_4^{2-}$ and electrical conductivity at 20.38–20.69 m (Figures 4B-1 and 4B-2), and we assigned these peaks to United States/St. Helens eruption in 1980 which was a volcanic explosivity index of 5. The Alaska/Katmai eruption in 1912 was the only eruption with a volcanic explosivity index of 6 in the high latitudes of the Northern Hemisphere during the twentieth century. The impact of Alaska/Katmai eruption was found as high electrical conductivity, SO$_4^{2-}$, and Cl$^-$ signals of some arctic ice cores (Cole-Dai et al., 2018; Coulter et al., 2012; Lyons et al., 1990; Tsushima et al., 2015; Yalcin et al., 2003). Extreme peaks of electrical conductivity and a Cl$^-$/Na$^+$ peak were found during 56.03–56.14 m (Figures 5D-2 and 5D-3). A high nssSO$_4^{2-}$ peak was found in 55.30–55.35 m after a winter from electrical conductivity and Cl$^-$/Na$^+$ peaks (Figure 5D-1). We assigned these peaks to the Alaska/Katmai eruption in 1912
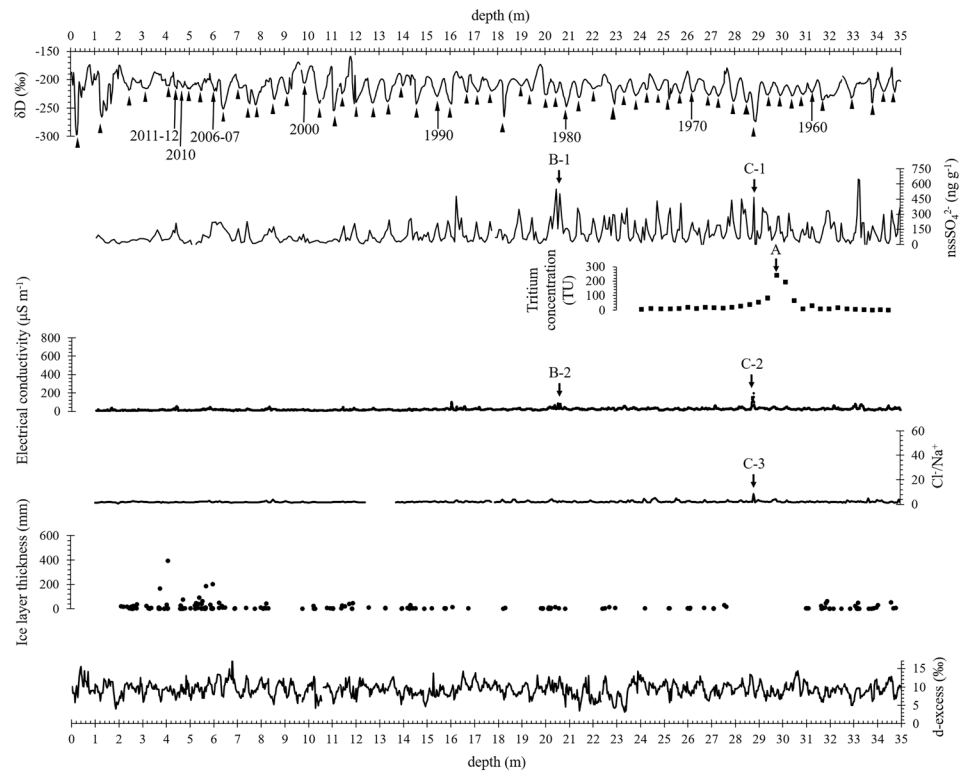

Figure 4. The vertical profile of δD, non-sea-salt (nss) SO$_4^{2-}$, tritium concentration (TU), electrical conductivity (DEP), Cl$^-$/Na$^+$, ice layer thickness, and d-excess in SIGMA-A ice core. The point marked A is the peak of H-bomb testing in 1963.
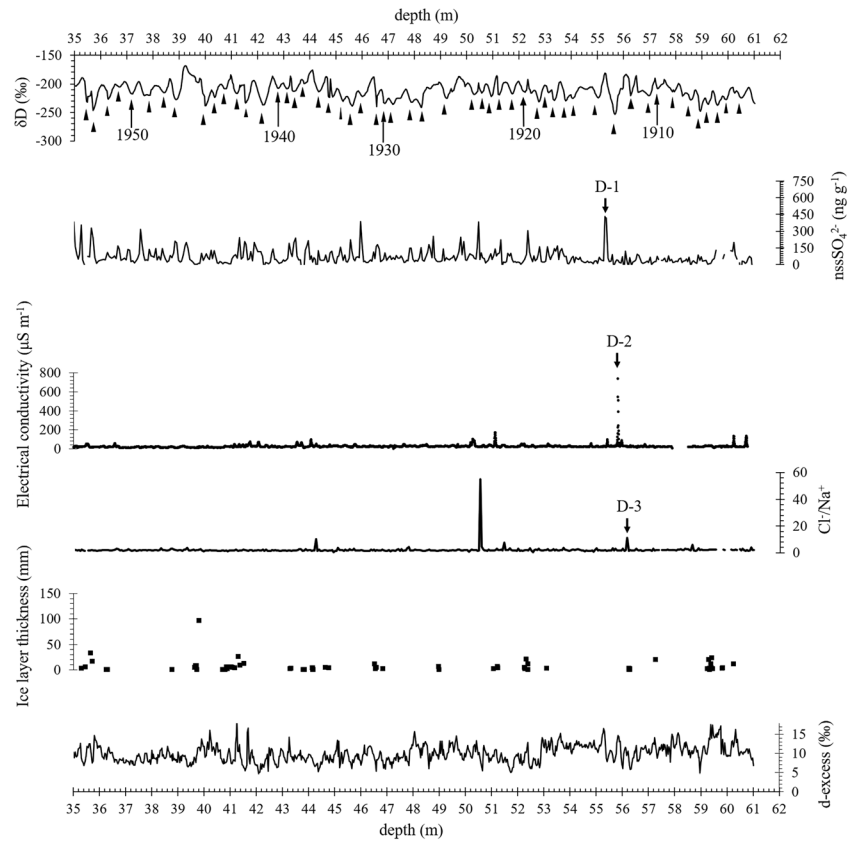
Figure 5. The vertical profile of δD, nssSO$_4^{2-}$, electrical conductivity (DEP), Cl$^-$/Na$^+$, ice layer thickness, and d-excess in SIGMA-A ice core.

(Figures 5D-2 and 5D-3). There was another peak of electrical conductivity, nssSO$_4^{2-}$, and Cl$^-$/Na$^+$ in a slightly shallower than tritium concentration peak in 1963 (Figures 4C-1, 4C-2, and 4C-3). It might be the peak appeared by Indonesia/Agung eruption. Herron (1982) mentioned that near-equatorial volcanic events
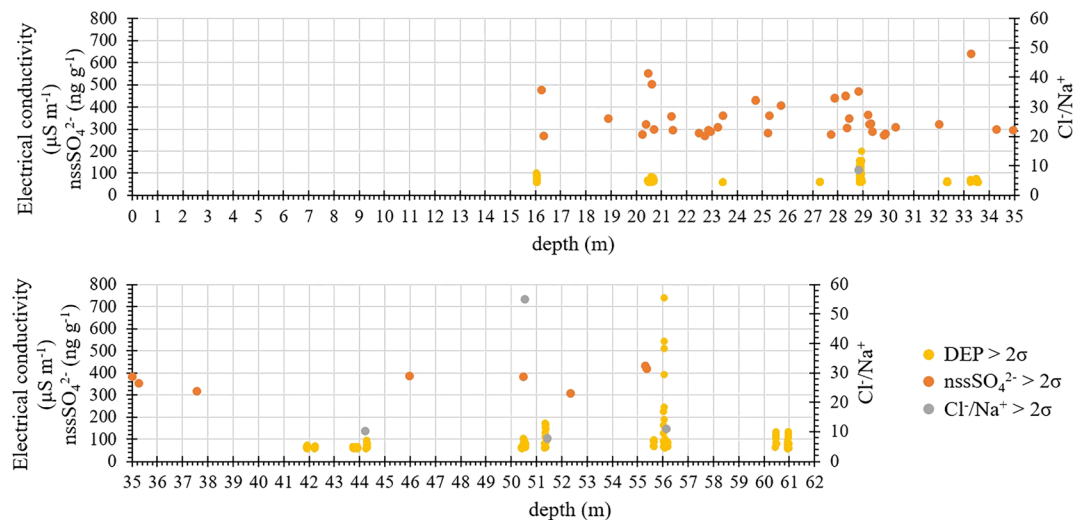

Figure 6. Peak values of electrical conductivity, nssSO$_4^{2-}$, and Cl$^-$/Na$^+$. Each peak was significantly large due to use standard deviation (>2σ).
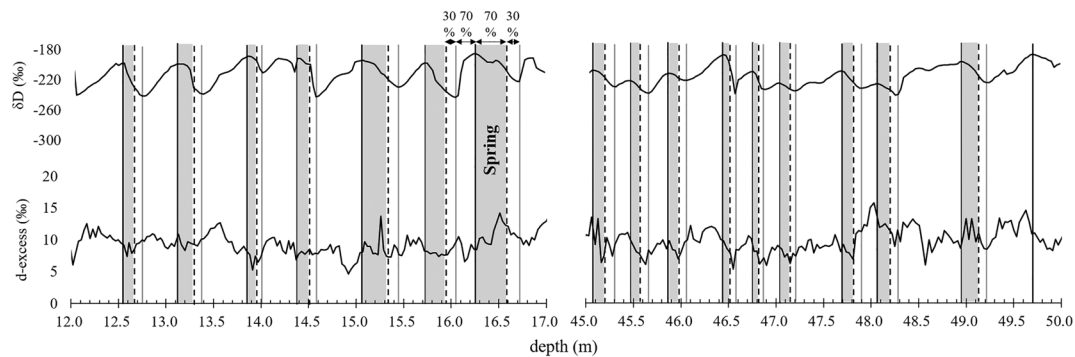
Figure 7. A schematic of estimations of spring layers in SIGMA-A ice core. Above and under graphs are vertical profiles (left side is during 12.0–16.5 m and right side is during 45.0–50.0 m) of δD and d-excess, respectively. A black and gray vertical solid line are positive peak depths and negative peak depths of δD, respectively. A black vertical dotted line are the depths corresponding to 70% from a positive peak to a negative peak of downward. A gray shade are spring layers.

have been shown in arctic ice core about 2 or 3 years later. Actually, volcanic peak of Agung eruption in NEEM ice core was found in 1963.9–1964.7 (Sig et al., 2013). Therefore, we assigned the peaks of electrical conductivity, $nssSO_4^{2-}$, and Cl^-/Na^+ to a volcanic eruption of Agung in 1963.

The annual layers of δD and Cl^-/Na^+ were counted manually above and below the reference horizons of the H-bomb test and the United States/St. Helens and Alaska/Katmai eruption. However, seasonal cycles of δD and Cl^-/Na^+ above 6.06 m were not clear because of the influence of meltwater. Therefore, we omitted the data above 6.06 m depth and used the data only from 6.06 to 61.06 m corresponding to 2005–1903 for reconstruction of past sea ice variations.

We identified the seasons in the ice core based on the ratio of precipitation amount in each season. The ratios of precipitation during October–March and April–September to total annual precipitation at SIGMA-A calculated with the ERA-interim daily precipitation data set from 1979–2005 were approximately 30% and 70%, respectively (Figure S2). A summer layer was defined as a layer of 70% from a positive peak to both a negative upward peak and a negative downward peak, and a winter layer was defined as a layer of 30% from a negative peak to both a positive upward peak and a positive downward peak. A spring layer was defined as a layer of 70% from a positive peak to a negative downward peak (Figure 7). Year by year changes in annual and spring means of d-excess are indicated in Figure 8.

To interpret variations of $\delta^{18}O$, δD, and d-excess in ice cores quantitatively, it is needed to evaluate post depositional changes of $\delta^{18}O$ and δD by water molecule diffusion in firn pore space and nonequilibrium effect on d-excess values in water vapor during atmospheric transportation from water vapor sources. The water molecule diffusion in firn pore space decrease amplitudes of seasonal variation of $\delta^{18}O$ and δD with
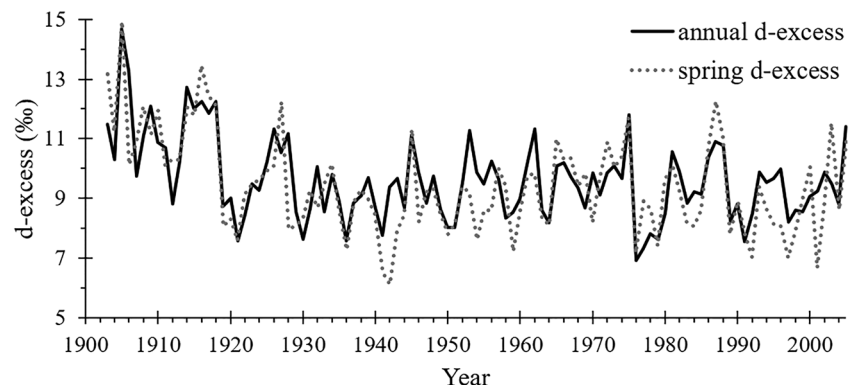

Figure 8. Interannual variations in d-excess for the annual mean (during pre-summer and the summer) (black) and spring mean (gray) during 1903–2005.

depth (Johnsen et al., 2000; Steen-Larsen et al., 2011). In SIGMA-A ice core, the decreases of the amplitude of $\delta^{18}O$ and δD were observed in deeper part (Figure S4). Changes of d-excess by the water molecule diffusion in firn pore space can be caused by difference of diffusion length between $\delta^{18}O$ and δD. According to Johnsen et al. (2000), we calculated the changes of d-excess by the water molecule diffusion in the SIGMA-A ice core (Figure S5). Consequently, the changes of d-excess were not significant in SIGMA-A ice core. Although it was possible that peaks of d-excess in deeper side of an ice core also shifted because of water molecular diffusion, the shifts of d-excess were not significant in SIGMA-A ice core (Figure 7). Therefore, the changes of d-excess by water molecule diffusion were negligible to following discussion.

To evaluate influence of changes of d-excess during transportation, we calculated exponential d-excess, which keep the influence of the nonequilibrium effect during ice and mixed-phase cloud formation and completely avoid the unphysical δ-scale effect (Dütsch et al., 2017). The calculated exponential d-excess of SIGMA-A ice core correlated with measured d-excess significantly ($r = 0.79$, $p < 0.001$). Therefore, we concluded that any influences of the nonequilibrium effect on d-excess values be negligible in this paper, in which only relative variation of d-excess was used to reconstruct the variation of sea ice concentration.

To obtain the annual accumulation rate, the depth was resampled at 1-year intervals based on the δD minima during 1903–2005. The depth of a 1-year interval indicates the annual accumulation rate in snow/ice equivalents. Then, the snow/ice accumulation rate in water-equivalent depth was calculated via multiplying by snow/ice density.

3.2. Moisture Source and Accumulation at SIGMA-A

To investigate the factors controlling the variations in water stable isotopes in the ice core, we estimated the moisture source for precipitation at SIGMA-A using LMSD. Figure 9 shows the uptake amount from the moisture source region transported toward SIGMA-A in each season during 1979–2016. The moisture uptake from Baffin Bay was largest in summer and smallest in winter. The seasonality of the moisture uptake was consistent with the seasonality of precipitation amounts at SIGMA-A. The moisture uptake in summer occurred across the whole area of northern Baffin Bay, and the contributions from NOW and the eastern area of Baffin Bay were remarkable. The dominant area of moisture uptake in spring and autumn was the eastern area of Baffin Bay. The WGC flows northward along the west coast of Greenland and prevents sea ice from moving toward the eastern part of Baffin Bay (Cuny et al., 2005). Therefore, the sea ice concentration in the eastern area of Baffin Bay is relatively low (Seidenkrantz, 2013), and the uptake amount of moisture from the area is higher than in other areas in spring and autumn.

Sodemann et al. (2008) reported that the moisture sources for precipitation at inland portions of the Greenland Ice Sheet were remote areas such as the Atlantic Ocean, Labrador Sea, and southern half of Baffin Bay. At the NEEM site (77°26′55″N, 51°03′20″W, 2,484 m a.s.l.), dominant moisture source for the snow deposited was assumed to be as far south as 35°N in the western part of the Atlantic Ocean (Steen-Larsen et al., 2011). On the other hand, we assume that the moisture source for precipitation at SIGMA-A is closer than those at inland areas; this source is the northern part of Baffin Bay because of the location of SIGMA-A, which is close to the ocean and at low elevation. Recently, Nusbaumer et al. (2019) argue that a significant proportion of moisture for the northwest ice sheet can be sourced from land snow and ice in the summer months. Although we do not discuss further on this point in the present study, it is necessary for us to investigate its effect utilizing the SIGMA-A Automated Weather Station (AWS) data as well as the recently developed high-resolution (5 km) nonhydrostatic polar regional climate model NHM-SMAP (Non Hydrostatic Model-Snow Metamorphism and Albedo Process) (Niwano et al., 2018).

Figure 10 shows the 5-year running mean (an annual mean was averaged during January–December) of the annual accumulation rate at the SIGMA-A ice core and the average moisture uptake in the northern part of Baffin Bay (70–78°N; 55–78°W) during 1981–2003. The annual accumulation rate at SIGMA-A correlates with the moisture uptake in the northern part of Baffin Bay ($r = 0.53$, $p < 0.01$). Consequently, the variations in the stable isotopes of water in the SIGMA-A ice core are reflected by environmental changes in local areas, such as the northern part of Baffin Bay, rather than changes in remote areas.

3.3. Reconstruction of Past Sea Ice Concentration

Evaporated water containing high d-excess diffuses into the atmosphere due to strong kinetic fractionation under such conditions as low relative humidity, high SST, and strong wind (Bonne et al., 2014; Steen-Larsen
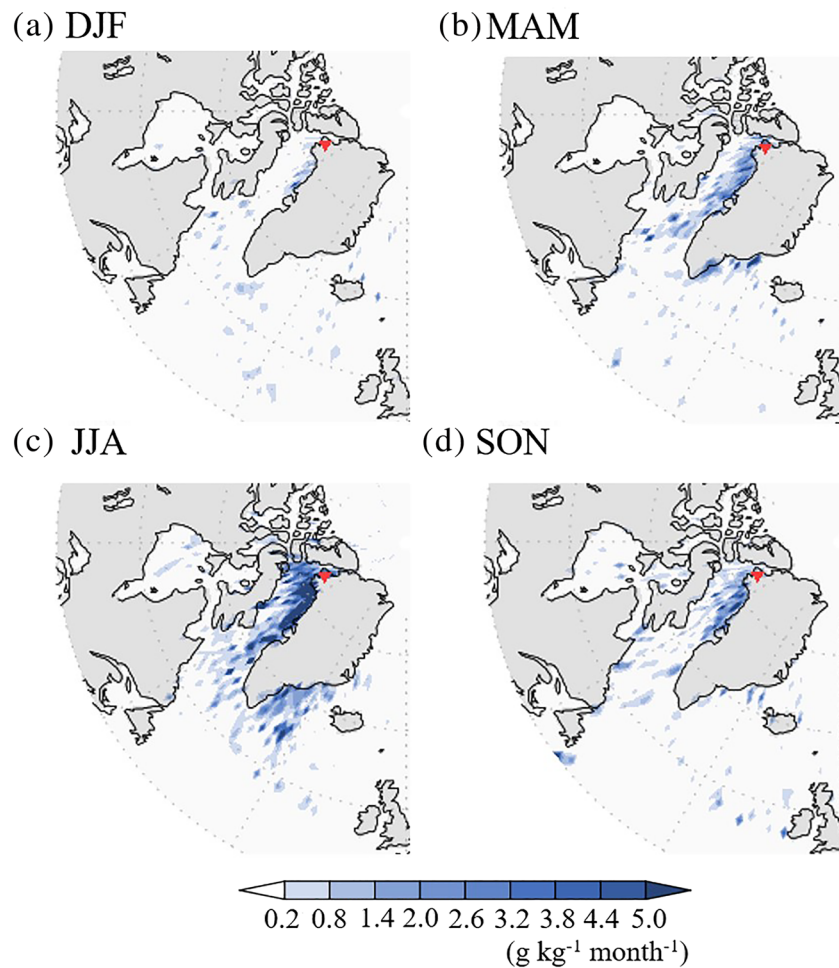
(a) DJF   (b) MAM

(c) JJA   (d) SON

0.2 0.8 1.4 2.0 2.6 3.2 3.8 4.4 5.0
(g kg^{-1} month^{-1})

Figure 9. Distributions of the amount of moisture uptake to the atmosphere transported toward SIGMA-A in (a) December–February, (b) March–May, (c) June–August, and (d) September–November during 1979–2016. Red inverted triangles indicate the position of SIGMA-A.

et al., 2014; Uemura et al., 2008). The variations in sea ice extent and concentration can influence these meteorological conditions in polar regions (Klein & Welker, 2016). Kurita (2011) suggested that evaporated water containing high d-excess was supplied to the atmosphere over the open water region surrounded by sea ice due to strong temperature contrasts between surface air temperature (SAT) and SST. Kurosaki et al. (2018) showed that the air masses leading to high d-excess snowfall were transported toward SIGMA-A via above the open water area. Therefore, d-excess in ice cores could indicate long-term variations in sea ice conditions because d-excess in precipitation in polar regions is affected by variations in sea ice conditions.

Figure 11 shows the scatter plot between annual or seasonal mean of sea ice concentration in the northern part of Baffin Bay and annual or seasonal mean of d-excess during 1979–2005. There was relatively high negative correlation between year-by-year variation in the northern part of Baffin Bay of sea ice concentration averaged from February to April and year-by-year variation of annual mean of d-excess ($r = -0.53$, $p < 0.01$) (Figure 11d). Therefore, we focused on the relationship between spring mean of d-excess and winter-spring mean of sea ice concentration. To extract the information about the environment in spring, the spring mean of d-excess was calculated from spring layers according to the definition described in section 3.1 (Figure 7). The SIGMA-A year-by-year variation of spring mean of d-excess is strongly correlated with the year-by-year variation of the northern part of Baffin Bay sea ice concentration averaged from February to April ($r = -0.61$, $p < 0.001$) (Figures 12c and 13a).
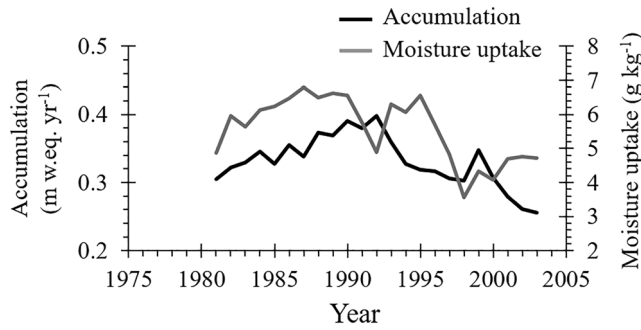
Figure 10. Profiles of 5-year running means of annual accumulation at SIGMA-A reconstructed from the SIGMA-A ice core (black) and annual mean of moisture uptake in the northern part of Baffin Bay (gray) during 1981–2003.

A single regression model incorporating the spring mean of d-excess in the SIGMA-A ice core explains 39% of the sea ice concentration in the northern part of Baffin Bay from winter to spring (February–April) ($SIC_{win.-spr.} = -0.55$ d-excess$_{spr.}$ + 74.73). Figure 14a shows the reconstructed values of the winter-spring mean of sea ice concentration around the northern part of Baffin Bay ($SIC_{win.-spr.}$) from 1903 to 2005 using the single regression model. Because the relationship between d-excess and sea ice concentration in spring still contains 60% of the variance unexplained by this relationship, there might be additional factors varying the d-excess of precipitation such as changes of dominant source regions of moisture, SST at moisture source, and so on. We believe that the most dominant factor is sea ice concentration, but we might evaluate possibilities of the other factors on discussions about reconstruction of past environment.

Sinclair et al. (2014) also found the negative correlation between d-excess in a coastal ice core obtained in Antarctica and sea ice area in the Ross Sea ($r = -0.53$, $p < 0.01$). The Ross Sea is formed polynya, and the size is directly linked to the strength of southerly winds transporting sea ice toward northward into the Ross Sea. The Ross Sea Polynya is increased by strong southerly wind. Therefore, the proportion of the water vapor with low d-excess for the precipitation nearby the Whitehall glacier which is the ice core drilling site is increased.

In contrast, Osterberg et al. (2015) found a positive correlation between the sea ice concentration in Baffin Bay and the annual d-excess in an ice core obtained from the northwestern Greenland Ice Sheet (2Barrel site). This study suggests the mechanism of a positive correlation between the sea ice concentration in Baffin Bay and the d-excess in the ice core. When Baffin Bay is covered with a high concentration of sea ice, the ratio of water vapor supplied from Baffin Bay to the 2Barrel site becomes low and that from the middle latitude area becomes relatively high. Because the d-excess of water vapor from middle latitudes, where SST is high, is generally high, the d-excess of precipitation should be high when the sea ice concentration in
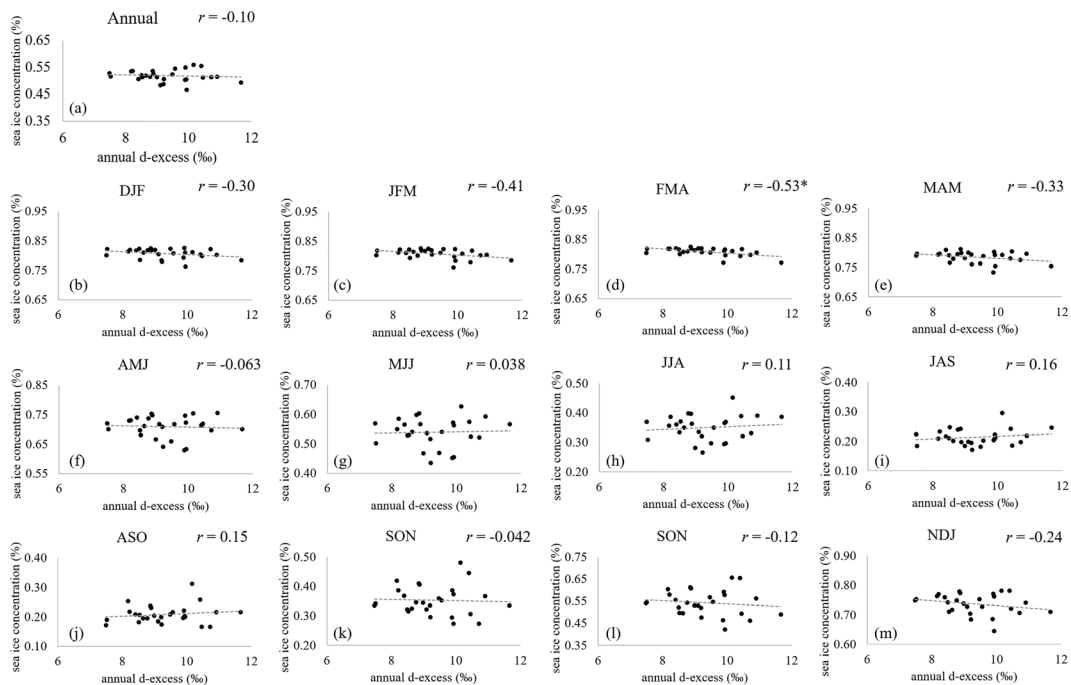

Figure 11. Scatter plots between sea ice concentration on annual (a) and each season (b–m) (3 months running mean) in the northern part of Baffin Bay and annual mean of d-excess from SIGMA-A ice core. The r shows Pearson correlation coefficient and the asterisk shows that p-value is less than 0.01. Each season are shown initial of month (e.g., DJF = December, January, and February).
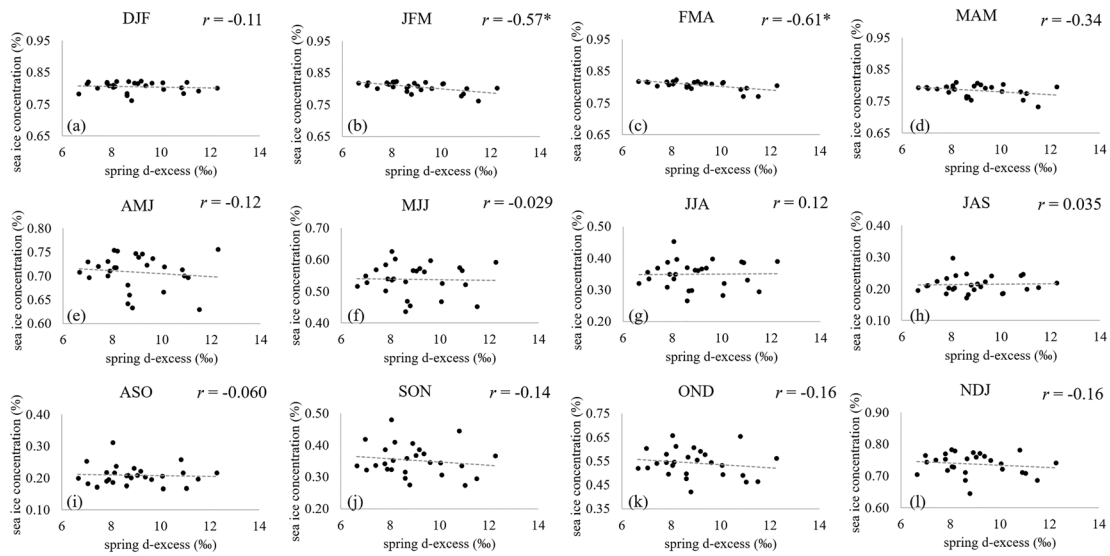
Figure 12. Scatter plots between sea ice concentration on each season (3 months running mean) in the northern part of Baffin Bay and spring mean of d-excess from SIGMA-A ice core. The *r* shows Pearson correlation coefficient and the asterisk shows that *p*-value is less than 0.01. Each season are shown initial of month (e.g., DJF = December, January and February).
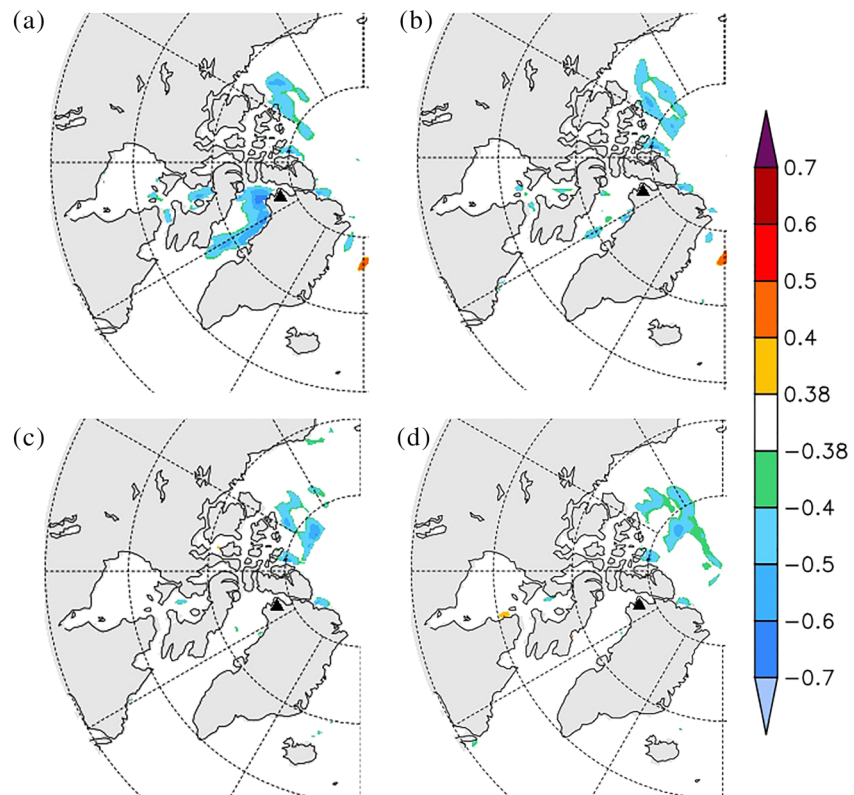

Figure 13. Spatial Pearson correlation maps between spring mean of d-excess in the SIGMA-A ice core and February–April (a), March–May (b), April–June (c), and May–July (d) mean sea ice concentrations during 1979–2005. The colored areas indicate that the correlation coefficient of a grid cell is statistically significant ($|r| > 0.38$, $p < 0.05$).
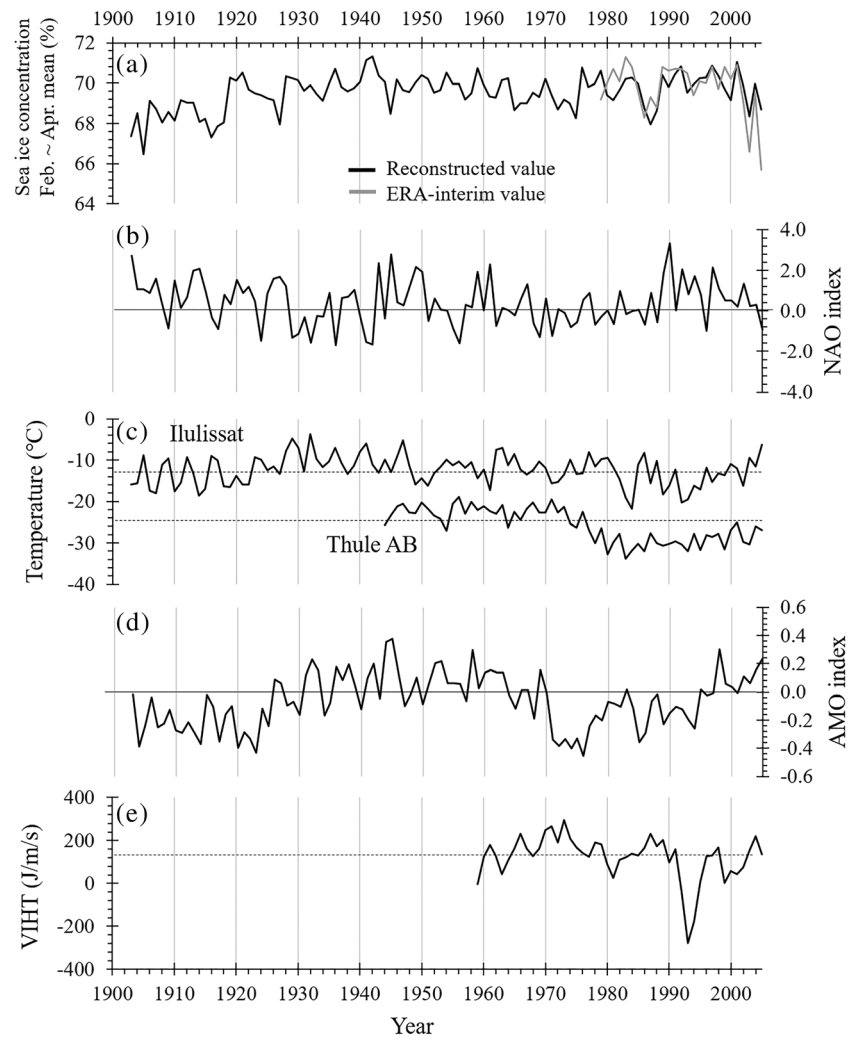
Figure 14. (a) Reconstructed sea ice concentration in the northern part of Baffin Bay in winter-spring (black line) and sea ice concentration in the northern part of Baffin Bay extracted from the ERA-interim reanalysis data set (gray line). (b) Average NAO index in February–April. (c) Average instrumental air temperature in February–April in Ilulissat and Thule Air Base. Dashed lines indicate the average temperature from 1903 to 2005. (d) Average AMO index in February–April. (e) Meridional component of vertically integrated heat transport through the area in 60–61°N and 48–54°W. Dashed lines indicate the average values from 1959 to 2005.

Baffin Bay is high. Kopec et al. (2016) also indicated that annual average of d-excess from some Canadian arctic region had positive correlation with sea ice extent of the Baffin Bay (60–80°N; 50–80°W), and other Greenland sites were indicated same positive correlation between sea ice and d-excess measured from precipitation or water vapor on the seasonal or year scale (Bonne et al., 2014; IAEA, 2014; Kopec et al., 2019).

We speculate that one of the most important reasons to explain the differences of interpretation of d-excess between this research and previous studies is a difference of locations of the observation sites and a source regions of water vapor transported to observation site. The elevation of the SIGMA-A site (1490 m a.s.l.) is comparable to that of the 2Barrel site (1685 m a.s.l.), but the distance from the SIGMA-A site to the coast of Greenland (30 km) is shorter than that from the 2Barrel site (~100 km). Moreover, the south side of the 2Barrel site faces to the Baffin Bay directly. Therefore, the precipitation at SIGMA-A site seems to be affected from closer area than the 2Barrel site. Thus, we estimated spatial distributions of amount of moisture uptake to atmosphere transported toward 2Barrel and SIGMA-A in annual and spring in 1996 and 2003 when annual sea ice concentration was relatively high and low, respectively (Figure 15). D-excess values in annual and in spring at SIGMA-A site were relatively low and high in 1996 and 2003, respectively (Figure 8).
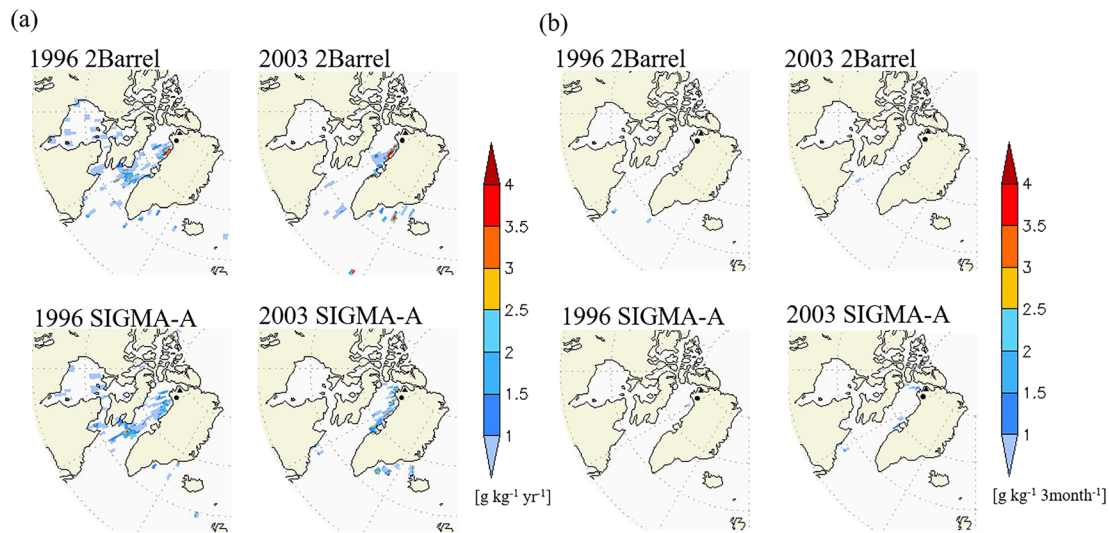
Figure 15. Distributions of amount of moisture uptake to atmosphere transported toward 2Barrel (above figures) and SIGMA-A (under figures) annual (a) or spring (b) precipitation in 1996 and 2003. Black triangles are SIGMA-A site and black circles are 2Barrel site.

Dominant areas of vapor source for precipitation in annual in SIGMA-A were the northern part of Baffin Bay and NOW in both of 1996 and 2003. Dominant areas of vapor source for precipitation in spring in SIGMA-A were NOW. On the other hand, dominant areas of vapor source for precipitation in annual and spring in 2Barrel were more southern area of the Baffin Bay. The estimated source area for 2Barrel is consistent with the speculated source area in Osterberg et al. (2015). Moreover, it is also consistent with the estimation of source areas for precipitations in SIGMA-A and 2Barrel that d-excess values in SIGMA-A ice core were lower in 2Barrel ice core. Because SST in more southern area is higher and d-excess of water vapor from high SST ocean tends to be high.

Sodemann et al. (2008) showed the moisture source for central west Greenland precipitation were north Atlantic Ocean and the southern part of Baffin Bay which was southern sea ice edge in NAO negative phase. At the NEEM site (2484 m a.s.l.), dominant moisture source for the snow deposited was assumed to as far south as 35°N from the western part of Atlantic Ocean (Steen-Larsen et al., 2011). Consequently, we speculated a reason why d-excess in the ice core at only SIGMA-A negatively correlated with sea ice concentration is that NOW can supply water vapor to SIGMA-A and not to other sites.

We speculate the mechanisms that d-excess in late winter and early spring in the ice core at SIGMA-A negatively correlated with sea ice concentrations as follows: in late winter and early spring, cold and dry air mass is transported from north of Greenland to the northern part of Baffin Bay by a wind of cyclonic flow. Water vapor is supplied to atmosphere from intervening open water of sea ice in the northern part of Baffin Bay driven by strong contrast of relative humidity between cold-dry air and air directly above the ocean. D-excess of the water vapor becomes high owing to the strong contrast of relative humidity. If the concentration of sea ice in source area of water vapor is low, that is the area of intervening open water is high, amount of water vapor with high d-excess supplied to atmosphere becomes high, and d-excess of precipitation becomes high.

3.4. Sea Ice Reduction in Early Twentieth Century

Figure 14a shows the reconstructed values of $SIC_{win.-spr.}$. The average values of $SIC_{win.-spr.}$ in the northern part of Baffin Bay during 1903–1920 and 1921–2005 were 68.45% and 69.74%, respectively. The $SIC_{win.-spr.}$ from 1903–1920 was significantly lower than that from 1921–2005 ($p < 0.01$). Grumet et al. (2001) reconstructed temporal variations in spring sea ice extent at Baffin Bay using sea-salt concentrations in an ice core drilled from Penny Ice Cap on Baffin Island and showed that spring sea ice extent was relatively low from the eighteenth to the early twentieth century. Cormier et al. (2016) also reconstructed the temporal variations in
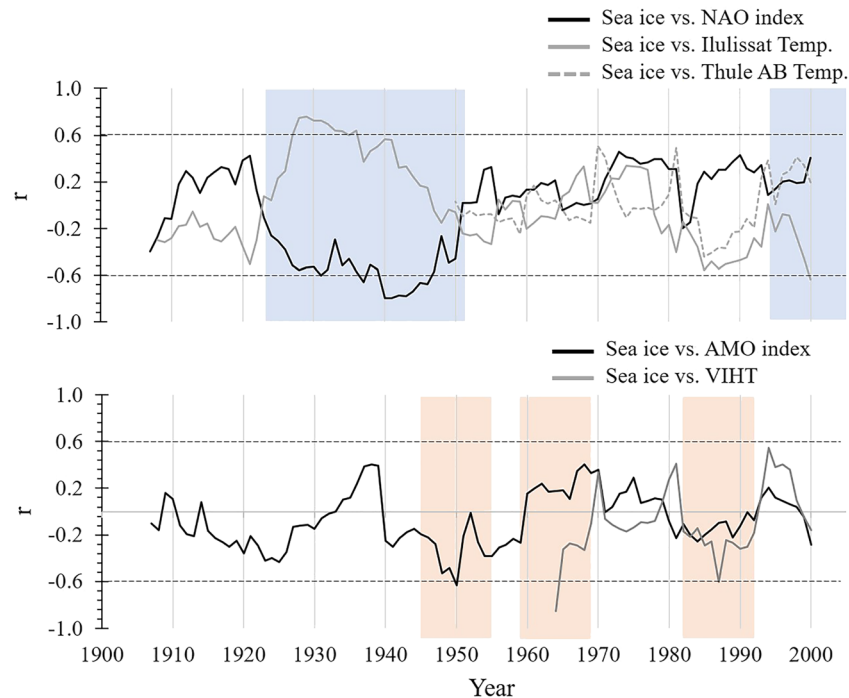
Figure 16. Displacement Pearson correlation coefficient for 11 years between winter-spring mean sea ice concentration in the northern part of Baffin Bay and (a) average NAO index in February–April and the instrumental air temperature of Ilulissat (a; gray line) and Thule air base (a; gray dotted line), (b) average AMO index in February–April and meridional component of vertically integrated heat transport through the area in 60–61°N and 48–54°W. The dashed line indicates the statistically correlated value ($|r| > 0.60$, $p < 0.05$). The blue band in (a) is the period of significant correlation between sea ice concentration and NAO index or air temperature in Ilulissat ($|r| > 0.60$, $p < 0.05$), and the red band in (b) is the period of significant correlation between sea ice concentration and AMO index or VIHT ($|r| > 0.60$, $p < 0.05$).

sea ice cover using marine sediments obtained from northern Baffin Bay and showed that the sea ice cover decreases from 9 to 7 months $year^{-1}$ between 1880 and 1915. These decreasing trends are consistent with our results. Generally, the SAT in the Northern Hemisphere from the sixteenth to the middle of the eighteenth century was low, and the period is called the Little Ice Age (LIA). In the Arctic region, SAT was still low after the LIA to the 1910s until the SAT dramatically increased in the 1920s (Shindell & Faluvegi, 2009). The instrumental record at Ilulissat in central western Greenland also showed that the Ilulissat SAT before 1920 was lower than that from 1921–1950 (Figure 14c). In western Greenland in the early twentieth century (1900–1910), the sea ice extent in Baffin Bay was low despite low SAT. We believe that the reduction of sea ice in the northern part of Baffin Bay in the early twentieth century was not controlled simply by changes in SAT but by complicated meteorological and/or oceanographic conditions.

Two of the indices indicating meteorological and oceanographic conditions around Greenland are the NAO index and AMO index, respectively. The NAO index corresponds to the development of the Icelandic low and northerly wind in northwestern Greenland. The AMO index corresponds to the SST of the North Atlantic Ocean. Figures 14b and 14d show the year-by-year variations in the NAO and AMO indices. In the early twentieth century, the NAO index was high, and the AMO index was low. Generally, when the NAO index is high, the sea ice concentration in Baffin Bay becomes high due to strong northerly wind blowing through Smith Sound under present conditions (Mysak et al., 1996; Stern & Heide-jørgensen, 2003). In this study, the NAO index was in a positive phase, but SIC$_{win.-spr.}$ in the northern part of Baffin Bay was low in the early twentieth century (Figures 14a and 14b). The results from the marine sediment core showed that the SST in northern Baffin Bay was relatively high in the early twentieth century (Cormier et al., 2016), while the AMO index was low. This situation means that the high SST was not caused by the increase in SST in the Atlantic Ocean but by the increase in heat transport to western Greenland and NOW by the WGC. The high SST in the northern part of Baffin Bay might have caused melting of sea ice inflowing from Smith Sound to NOW during winter-spring in the early twentieth century.

3.5. The Mechanism of Year-by-Year Change in Sea Ice

During 1920–2005, the reconstructed values of $SIC_{win.-spr.}$ in the northern part of Baffin Bay show year-by-year variations. To reveal the mechanism of year-by-year variations in $SIC_{win.-spr.}$, we compare reconstructed $SIC_{win.-spr.}$ to the climate index (NAO) (Figure 14b), the instrumental air temperatures at Ilulissat and Thule Air Base, which is the meteorological data station nearest to the SIGMA-A site (Figure 14c), the oceanographic index (AMO) (Figure 14d) and the meridional component of vertically integrated heat transport (VIHT) in the region from 60–61°N and 48–54°W (Figure 14e). Figure 16a shows a displacement Pearson correlation coefficient for 11 years between $SIC_{win.-spr.}$ and the NAO index from February to April and air temperatures from February to April at Ilulissat and Thule Air Base. $SIC_{win.-spr.}$ correlated with NAO index negatively from 1926 to 1951 ($r = -0.60$, $p < 0.05$), with SAT at Ilulissat positively from 1922 to 1941 ($r = 0.60$, $p < 0.05$) and negatively from 1995 to 2005 ($r = -0.60$, $p < 0.05$) and did not correlate with SAT at Thule Air Base, the nearest meteorological data station to the SIGMA-A site. Polyakov et al. (2003) indicated that a positive NAO index induces stronger northerly wind and low SAT on the west coast of Greenland. On the other hand, in a negative NAO index, southerly wind is induced and brings warm and wet moisture including high d-excess from lower latitude (Kopec et al., 2016). In fact, the SAT at Ilulissat became high between the 1920s and 1950s when the NAO index was relatively low (Figures 14b and 14c). However, the spring mean of d-excess in SIGMA-A ice core were relatively low and the reconstructed $SIC_{win.-spr.}$ was high during the period. The SIGMA-A site locates on the northern peninsula behind the southern peninsula where the 2Barrel site and Tule Air Base are. Therefore, the moisture from lower latitude was scavenged at the southern peninsula and moisture which brings snowfall to the SIGMA-A site did not mix with the moisture from lower latitude. We speculate that the reason for the negative correlation between $SIC_{win.-spr.}$ and the NAO index from 1926–1951 can be described as follows: SAT in south and middle west Greenland remained high from late winter to early spring in the 1920s–1950s. When northerly wind blows strongly, corresponding to a high NAO index, the amount of sea ice transported toward the south in the early sea ice melting season increases, and the melting of sea ice is enhanced.

Figure 16b shows a displacement Pearson correlation coefficient between $SIC_{win.-spr.}$ and the AMO index and VIHT in February–April. $SIC_{win.-spr.}$ in the northern part of Baffin Bay was negatively correlated with the AMO index during 1945–1955 ($r = -0.60$, $p < 0.05$). In this period, $SIC_{win.-spr.}$ was controlled by SST in the north Atlantic Ocean flowing into Baffin Bay by the WGC. $SIC_{win.-spr.}$ also correlated negatively with VIHT during 1959–1969 and 1982–1992 ($r = -0.60$, $p < 0.05$). In these periods, increasing the inflow of warm water masses from the south promoted high SST and sea ice melting during the winter-spring in NOW. In fact, the high SST promoted diffusing of the water vapor, which included high d-excess, by strong evaporation. Therefore, it is possible that the d-excess of the moisture for snowfall in the SIGMA-A site was influenced by oceanographic circulation such as WGC and SST in NOW, directly.

Consequently, the factors controlling the sea ice concentration in the northern part of Baffin Bay varied temporally.

4. Conclusions

A 60.06 m ice core obtained from the SIGMA-A site, northwestern Greenland Ice Sheet, was analyzed for water stable isotopes and chemical species. We estimated the age of the ice core by counting the annual cycles of δD and Cl^-/Na^+ and using reference horizons of a tritium peak from the H-bomb test in 1963 and a peak from the volcanic eruptions of St. Helens in 1980 and Katmai in 1912 detected by DEP, $nssSO_4^{2-}$, and Cl^-/Na^+. The ice core covered from 1903 to 2017. We also estimated seasonal layers in each year using the seasonal cycle of δD and the seasonal distribution of precipitation at the SIGMA-A site estimated from reanalysis data. The temporal variations in d-excess in spring in the ice core correlated negatively and significantly with those of sea ice concentration in winter-spring (February–April) in the northern Baffin Bay in 1979–2005. Using this relationship, we reconstructed the temporal variations in the sea ice concentrations during winter-spring in Baffin Bay for approximately 100 years from the record of d-excess in the ice core. The reconstructed sea ice concentration showed that the sea ice concentrations were low in the early twentieth century. The period with low sea ice concentrations is consistent with the results from analyses of marine sediment obtained from northern Baffin Bay. After the period with low sea ice concentration, the sea ice concentration correlated negatively with the NAO index from 1926–1951

and positively with February–April air temperature in Ilulissat from 1922–1941. In this period, the air temperature in Ilulissat was relatively high, and we hypothesized that the sea ice concentration of Baffin Bay was mainly controlled by the meteorological conditions at this time. On the other hand, the sea ice concentration correlated negatively with the AMO index from 1945–1955 and with meridional heat transport to western Greenland from the south in 1959–1969 and 1982–1992. In these periods, the sea ice concentration in Baffin Bay was mainly controlled by oceanographic conditions in western Greenland, especially transport of heat by the WGC. In this study, it is possible that the oceanographic circulation affects the d-excess in the moisture for snowfall in the SIGMA-A site independently of sea ice concentration. Uncertainty of the relationship between d-excess in the SIGMA-A ice core and sea ice concentration in the northern part of Baffin Bay should be evaluated in the future study.

Data Availability Statement

The data used in this study will be available in Hokkaido University Collection of Scholarly and Academic papers (http://hdl.handle.net/2115/78834). The ERA-Interim data was provided courtesy of ECMWF (https://apps.ecmwf.int/datasets/data/interim-full-daily/levtype=sfc/). The NAO index data and the AMO index data were provided courtesy of University of East Anglia (https://crudata.uea.ac.uk/cru/data/nao/) and ESRL, NOAA (https://www.esrl.noaa.gov/psd/data/timeseries/AMO/), respectively. The 10-day backward trajectories were calculated by the HYSPLIT model provided by NOAA (https://www.ready.noaa.gov/HYSPLIT.php). The VIHT data were provided by ORA-S3, ECMWF (http://apdrc.soest.hawaii.edu/datadoc/ecmwf_oras3.php).

References

Aoki, T., Matoba, S., Uetake, J., Takeuchi, N., & Motoyama, H. (2014). Field activities of the "snow impurity and glacial microbe effects on abrupt warming in the Arctic" (SIGMA) project in Greenland in 2011-2013. *Bulletin of Glaciological Research*, *32*, 3–20. https://doi.org/10.5331/bgr.32.3

Balmaseda, M. A., Vidard, A., & Anderson, D. L. T. (2008). The ECMWF Ocean Analysis System: ORA-S3. *Monthly Weather Review*, *136*(8), 3018–3034. https://doi.org/10.1175/2008mwr2433.1

Bonne, J.-L., Masson-Delmotte, V., Cattani, O., Delmotte, M., Risi, C., Sodemann, H., & Steen-Larsen, H. C. (2014). The isotopic composition of water vapour and precipitation in Ivittuut, southern Greenland. *Atmospheric Chemistry and Physics*, *14*(9), 4419–4439. https://doi.org/10.5194/acp-14-4419-2014

Clausen, H. B., & Hammer, C. U. (1988). The Laki and Tambora eruptions as revealed in Greenland ice cores from 11 locations. *Annals of Glaciology*, *10*, 16–22. https://doi.org/10.1017/s0260305500004092

Cole-Dai, J., Peterson, K. M., Kennedy, J. A., Cox, T. S., & Ferris, D. G. (2018). Evidence of influence of human activities and volcanic eruptions on environmental perchlorate from a 300-year Greenland ice Core record. *Environmental Science Technology*, *52*(15), 8373–8380. https://doi.org/10.1021/acs.est.8b01890

Cormier, M. A., Rochon, A., de Vernal, A., & Gélinas, Y. (2016). Multi-proxy study of primary production and paleoceanographical conditions in northern Baffin Bay during the last centuries. *Marine Micropaleontology*, *127*, 1–10. https://doi.org/10.1016/j.marmicro.2016.07.001

Coulter, S. E., Pilcher, J. R., Plunkett, G., Baillie, M., Hall, V. A., Steffensen, J. P., et al. (2012). Holocene tephras highlight complexity of volcanic signals in Greenland ice cores. *Journal of Geophysical Research*, *117*, D21303. https://doi.org/10.1029/2012JD017698

Craig, H. (1961). Isotopic variation in meteoric waters. *Science*, *133*(3465), 1702–1703. https://doi.org/10.1126/science.133.3465.1702

Cuny, J., Rhines, P. B., & Kwok, R. (2005). Davis Strait volume, freshwater and heat fluxes. *Deep-Sea Research Part I: Oceanographic Research Papers*, *52*(3), 519–542. https://doi.org/10.1016/j.dsr.2004.10.006

Dansgaard, W. (1964). Stable isotopes in precipitation. *Tellus*, *16*(4), 436–468. https://doi.org/10.3402/tellusa.v16i4.8993

Dee, D. P., Uppala, S. M., Simmons, A. J., Berrisford, P., Poli, P., Kobayashi, S., et al. (2011). The ERA-interim reanalysis: Configuration and performance of the data assimilation system. *Quarterly Journal of the Royal Meteorological Society*, *137*(656), 553–597. https://doi.org/10.1002/qj.828

Dibb, J. E., Whitlow, S. l., & Arsenault, M. (2007). Seasonal variations in the soluble ion content of snow at Summit, Greenland: Constraints from three years of daily surface snow samples. *Atmospheric Environment*, *41*(24), 5007–5019. https://doi.org/10.1016/j.atmosenv.2006.12.010

Dumont, D., Gratton, Y., & Arbetter, T. E. (2009). Modeling the dynamics of the north water polynya ice bridge. *Journal of Physical Oceanography*, *39*(6), 1448–1461. https://doi.org/10.1175/2008jpo3965.1

Dütsch, M., Pfahl, S., & Sodemann, H. (2017). The Impact of Nonequilibrium and Equilibrium Fractionation on Two Different Deuterium Excess Definitions. *Journal of Geophysical Research: Atmospheres*, *122*, 12,732–12,746. https://doi.org/10.1002/2017JD027085

Enfield, D. B., Mestas-Nuñez, A. M., & Trimble, P. J. (2001). The Atlantic multidecadal oscillation and its relation to rainfall and river flows in the continental U.S. *Geophysical Research Letters*, *28*(10), 2077–2080. https://doi.org/10.1029/2000GL012745

Fujita, S., Goto-Azuma, K., Hirabayashi, M., Hori, A., Iizuka, Y., Motizuki, Y., et al. (2016). Densification of layered firn in the ice sheet at Dome Fuji, Antarctica. *Journal of Glaciology*, *62*(231), 103–123. https://doi.org/10.1017/jog.2016.16

Furukawa, R., Uemura, R., Fujita, K., Sjolte, J., Yoshimura, K., Matoba, S., & Iizuka, Y. (2017). Seasonal-scale dating of a shallow ice core from Greenland using oxygen isotope matching between data and simulation. *Journal of Geophysical Research: Atmospheres*, *122*, 10,873–10,887. https://doi.org/10.1002/2017JD026716

Gat, J. R. (1996). Oxygen and hydrogen isotopes in the hydrologic cycle. *Annual Review of Earth and Planetary Sciences*, *24*(1), 225–262. https://doi.org/10.1146/annurev.earth.24.1.225

Grumet, N. S., Wake, C. P., Mayewski, P. A., Zielinski, G. A., Whitlow, S. I., Koerner, R. M., et al. (2001). Variability of sea-ice extent in Baffin Bay over the last millennium. *Climatic Change*, *49*(1/2), 129–145. https://doi.org/10.1023/A:1010794528219

Herron, M. M. (1982). Impurity sources of F-, CI-, N03- and SO/- in Greenland and Antarctic precipitation. *Journal of Geophysical Research*, *87*(C4), 3052–3060. https://doi.org/10.1029/JC087iC04p03052

Hori, A., Tayuki, K., Narita, H., Hondoh, T., Fujita, S., Kameda, T., et al. (1999). A detailed density profile of the Dome Fuji (Antarctica) shallow ice core by X-ray transmission method. *Annals of Glaciology*, *29*, 211–214. https://doi.org/10.3189/172756499781821157

Hurrell, J. W. (1995). Decadal trends in the North Atlantic Oscillation: Regional temperatures and precipitation. *Science*, *269*(5224), 676–679. https://doi.org/10.1126/science.269.5224.676

IAEA. (2014). Global network of isotopes in precipitation. *GNIP database*.

Iizuka, Y., Miyamoto, A., Hori, A., Matoba, S., Furukawa, R., Saito, T., et al. (2017). A firn densification process in the high accumulation dome of southeastern Greenland. *Arctic, Antarctic, and Alpine Research*, *49*(1), 13–27. https://doi.org/10.1657/AAAR0016-034

James, P., Stohl, A., Spichtinger, N., Eckhardt, S., & Forster, C. (2004). Climatological aspects of the extreme European rainfall of August 2002 and a trajectory method for estimating the associated evaporative source regions. *Natural Hazards and Earth System Science*, *4*(5/6), 733–746. https://doi.org/10.5194/nhess-4-733-2004

Johnsen, S. J., Clausen, H. B., Cuffey, K. M., Hoffmann, G., Schwander, J., & Creyts, T. (2000). Diffusion of stable isotopes in polar firn and ice: The isotope effect in firn diffusion. *In Physics of ice core records*, 121–140.

Jones, P. D., Jonsson, T., & Wheeler, D. (1997). Extension to the North Atlantic oscillation using early instrumental pressure observations from Gibraltar and south-west Iceland. *International Journal of Climatology*, *17*(13), 1433–1450. https://doi.org/10.1002/(sici)1097-0088(19971115)17:13<1433::aid-joc203>3.0.co;2-p

Kerr, R. A. (2000). A North Atlantic climate pacemaker for the centuries. *Science*, *288*(5473), 1984–1985. https://doi.org/10.1126/science.288.5473.1984

Klein, E. S., & Welker, J. M. (2016). Influence of sea ice on ocean water vapor isotopes and Greenland ice core records. *Geophysical Research Letters*, *43*, 12,475–12,483. https://doi.org/10.1002/2016GL071748

Kopec, B. G., Feng, X., Michel, F. A., & Posmentier, E. S. (2016). Influence of sea ice on Arctic precipitation. *Proceeding of the National Academy of Sciences of the United Status of America*, *113*(1), 46–51. https://doi.org/10.1073/pnas.1504633113

Kopec, B. G., Feng, X., Posmentier, E. S., & Sonder, L. J. (2019). Seasonal deuterium excess variations of precipitation at summit, Greenland, and their climatological significance. *Journal of Geophysical Research: Atmospheres*, *124*, 72–91. https://doi.org/10.1029/2018JD028750

Kuramoto, T., Goto-azuma, K., Hirabayashi, M., Miyake, T., Motoyama, H., Dahl-jensen, D., & Steffensen, J. P. (2011). Seasonal variations of snow chemistry at NEEM, Greenland. *Annals of Glaciology*, *52*(58), 193–200. https://doi.org/10.3189/172756411797252365

Kurita, N. (2011). Origin of Arctic water vapor during the ice-growth season. *Geophysical Research Letters*, *38*, L02709. https://doi.org/10.1029/2010GL046064

Kurosaki, Y., Matoba, S., Iizuka, Y., Niwano, M., Tanikawa, T., & Aoki, T. (2018). Influence of environmental conditions near Baffin Bay on deuterium excess and chemical substances in falling snow in northwestern Greenland. *Journal of the Japanese Society of Snow and Ice*, *80*(6), 515–529. [in Japanese with English abstract]

Legrand, M., & Mayewski, P. (1997). Glaciochemistry of polar ice cores: A review. *Reviews of Geophysics*, *35*(3), 219–243. https://doi.org/10.1029/96RG03527

Lyons, W. B., Mayewski, P. A., Spencer, M. J., & Twickler, M. S. (1990). A northern hemisphere volcanic chemistry record (1869–1984) and climatic implications using a south Greenland ice core. *Annals of Glaciology*, *14*, 176–182. https://doi.org/10.3189/S0260305500008521

Matoba, S., & Yamasaki, T. (2018). Sea ice outflow damage to fishery in Qaanaaq, northwestern Greenland in December 2016—Changes of the livelihood associated with social and environmental changes. *Annual Report of Snow and Ice Sheet in Hokkaido*, *37*, 51–54. [in Japanese]

Matoba, S., Niwano, M., Tanikawa, T., Iizuka, Y., Yamasaki, T., Kurosaki, Y., et al. (2018). Field activities at the SIGMA-A site, northwestern Greenland Ice Sheet, 2017. *Bulletin of Glaciological Research*, *36*(0), 15–22. https://doi.org/10.5331/bgr.18r01

Matoba, S., Yamaguchi, S., Tsushima, A., Aoki, T., & Sugiyama, S. (2016). Surface mass balance variations in a maritime area of the northwestern Greenland Ice Sheet. *Low Temperature Science*, *75*, 37–44.

Matoba, S., Yamasaki, T., Miyahara, M., & Motoyama, H. (2014). Spatial variations of δ18O and ion species in the snowpack of the northwestern Greenland ice sheet. *Bulletin of Glaciological Research*, *32*(0), 79–84. https://doi.org/10.5331/bgr.32.79

Melling, H., Gratton, Y., & Ingram, G. (2001). Ocean circulation within the North Water polynya of Baffin Bay. *Atmosphere - Ocean*, *39*(3), 301–325. https://doi.org/10.1080/07055900.2001.9649683

Merlivat, L., & Jouzel, J. (1979). Global climatic interpretation of the deuterium-oxygen 16 relationship for precipitation. *Journal of Geophysical Research*, *84*(C8), 5029–5033. https://doi.org/10.1029/JC084iC08p05029

Minnett, P. J., & Key, E. L. (2007). Meteorology and atmosphere-surface coupling in and around polynyas. In W. O. Smith, & D. G. Barber (Eds.), *Polynyas: Windows to the world* (Vol. 74, pp. 127–154). Amsterdam: Elsevier. https://doi.org/10.1016/S0422-9894(06)74004-1

Moore, J. C., & Paren, J. G. (1987). A new technique for dielectric logging of Antarctic ice cores. *Journal of Physical Colloques*, *48*(C1), C1-155–C1-160. https://doi.org/10.1051/jphyscol:1987123

Mysak, L. A., Ingram, R. G., Wang, J., & Van Der Baaren, A. (1996). The anomalous sea-ice extent in Hudson bay, Baffin bay and the Labrador Sea during three simultaneous NAO and ENSO episodes. *Atmosphere - Ocean*, *34*(2), 313–343. https://doi.org/10.1080/07055900.1996.9649567

Niwano, M., Aoki, T., Hashimoto, A., Matoba, S., Yamaguchi, S., Tanikawa, T., et al. (2018). NHM–SMAP: Spatially and temporally high-resolution nonhydrostatic atmospheric model coupled with detailed snow process model for Greenland Ice Sheet. *The Cryosphere*, *12*(2), 635–655. https://doi.org/10.5194/tc-12-635-2018

Nusbaumer, J., Alexander, P. M., LeGrande, A. N., & Tedesco, M. (2019). Spatial Shift of Greenland Moisture Sources Related to Enhanced Arctic Warming. *Geophysical Research Letters*, *46*, 14,723–14,731. https://doi.org/10.1029/2019GL084633

Osterberg, E. C., Hawley, R. L., Wong, G., Kopec, B., Ferris, D., & Howley, J. (2015). Coastal ice-core record of recent northwest Greenland temperature and sea-ice concentration. *Journal of Glaciology*, *61*(230), 1137–1146. https://doi.org/10.3189/2015JoG15J054

Oyabu, I., Matoba, S., Yamasaki, T., Kadota, M., & Iizuka, Y. (2016). Seasonal variations in the major chemical species of snow at the South East Dome in Greenland. *Polar Science*, *10*(1), 36–42. https://doi.org/10.1016/j.polar.2016.01.003

Polyakov, I. V., Bekryaev, R. V., Alekseev, G. V., Bhatt, U. S., Colony, R. L., Johnson, M. A., et al. (2003). Variability and trends of air temperature and pressure in the maritime Arctic, 1875–2000. *Journal of Climate*, *16*(12), 2067–2077. https://doi.org/10.1175/1520-0442(2003)016<2067:VATOAT>2.0.CO;2

Ribergaard, M. H., Olsen, S. M., & Mortensen, J. (2008). Oceanographic investigations off West Greenland 2007. *NAFO Scientific Council Research Document*, *08*(3), 1–51.

Seidenkrantz, M. (2013). Benthic foraminifera as palaeo sea-ice indicators in the subarctic realm – examples from the Labrador Sea–Baffin Bay region. *Quaternary Science Reviews*, *79*, 135–144. https://doi.org/10.1016/j.quascirev.2013.03.014

Shindell, D., & Faluvegi, G. (2009). Climate response to regional radiative forcing during the twentieth century. *Nature Geoscience*, *2*(4), 294–300. https://doi.org/10.1038/ngeo473

Shiraiwa, T., Kanamori, S., Benson, C. S., Solie, D., & Muravyev, Y. D. (2004). Shallow ice-core drilling at Mount Wrangell, Alaska. *Bulltein of Glaciological Research*, *21*, 71–77.

Sig, M., McConnell, J. R., Layman, L., Maselli, O., McGwire, K., Pasteris, D., et al. (2013). A new bipolar ice core record of volcanism from WAIS Divide and NEEM and implications for climate forcing of the last 2000 years. *Journal of Geophysical Research*, *118*, 1151–1169. https://doi.org/10.1029/2012JD018603

Sinclair, K. E., Bertler, N. A. C., Bowen, M. M., & Arrigo, K. R. (2014). Twentieth century sea-ice trends in the Ross Sea from a high-resolution, coastal ice-core record. *Geophysical Research Letters*, *41*, 3510–3516. https://doi.org/10.1002/2014GL059821

Sodemann, H., Schwierz, C., & Wernli, H. (2008). Interannual variability of Greenland winter precipitation sources: Lagrangian moisture diagnostic and North Atlantic Oscillation influence. *Journal of Geophysical Research*, *113*, D03107. https://doi.org/10.1029/2007JD008503

Steen-Larsen, H. C., Masson-Delmotte, V., Sjolte, J., Johnsen, S. J., Vinther, B. M., Bréon, F.-M., et al. (2011). Understanding the climatic signal in the water stable isotope records from the NEEM shallow firn/ice cores in northwest Greenland. *Journal of Geophysical Research*, *116*, D06108. https://doi.org/10.1029/2010JD014311

Steen-Larsen, H. C., Sveinbjörnsdottir, A. E., Peters, A. J., Masson-Delmotte, V., Guishard, M. P., Hsiao, G., et al. (2014). Climatic controls on water vapor deuterium excess in the marine boundary layer of the North Atlantic based on 500 days of in situ, continuous measurements. *Atmospheric Chemistry and Physics*, *14*(15), 7741–7756. https://doi.org/10.5194/acp-14-7741-2014

Stein, A. F., Draxler, P. R., Rolph, G. D., Stunder, B. J. B., Cohen, M. D., & Ngan, F. (2015). NOAA's HYSPLIT atmospheric transport and dispersion modeling system. *Bulletin of the American Meteorological Society*, *96*(12), 2059–2077. https://doi.org/10.1175/bams-d-14-00110.1

Stern, H. L., & Heide-jørgensen, M. P. (2003). Trends and variability of sea ice in Baffin Bay. *Applied Physics*, *22*(1), 11–18. https://doi.org/10.3402/polar.v22i1.6438

Stohl, A., & James, P. (2004). A Lagrangian analysis of the atmospheric branch of the global water cycle. Part I: Method description, validation, and demonstration for the August 2002 flooding in Central Europe. *Journal of Hydrometeorology*, *5*, 656–678. https://doi.org/10.1175/1525-7541(2004)005<0656:ALAOTA>2.0.CO;2

Tsushima, A., Matoba, S., Shiraiwa, T., Okamoto, S., Sasaki, H., Solie, D. J., & Yoshikawa, K. (2015). Reconstruction of recent climate change in Alaska from the Aurora Peak ice core, central Alaska. *Climate of the Past*, *11*(2), 217–226. https://doi.org/10.5194/cp-11-217-2015

Uemura, R., Matsui, Y., Yoshimura, K., Motoyama, H., & Yoshida, N. (2008). Evidence of deuterium excess in water vapor as an indicator of ocean surface conditions. *Journal of Geophysical Research*, *113*, D19114. https://doi.org/10.1029/2008JD010209

Wilhelms, F., Kipfstuhl, J., Miller, H., Heinloth, K., & Firestone, J. (1998). Precise dielectric profiling of ice cores: A new device with improved guarding and its theory. *Journal of Glaciology*, *44*(146), 171–174. https://doi.org/10.3189/S002214300000246X

Wilson, T. R. S. (1975). Salinity and the major elements of sea water. In J. P. Riley & G. Skittow (Eds.), *Chemical Oceanography* (Vol. 1, pp. 365–413). London: Academic Press.

Yalcin, K., Cameron, P. W., & Germani, M. S. (2003). A 100-year record of North Pacific volcanism in an ice core from Eclipse Icefield, Yukon Territory, Canada. *Journal of Geophysical Research*, *108*(D1), 4012. https://doi.org/10.1029/2002JD002449

Yamaguchi, S., Matoba, S., Yamazaki, T., Tsushima, A., Niwano, M., Tanikawa, T., & Aoki, T. (2014). Glaciological observations in 2012 and 2013 at SIGMA-A site, Northwest Greenland. *Bulletin of Glaciological Research*, *32*(0), 95–105. https://doi.org/10.5331/bgr.32.95

References From the Supporting Information

Herron, M. M., & Langway, C. C. (1980). Firn densification: An empirical model. *Journal of Glaciology*, *25*(93), 373–385. https://doi.org/10.3189/S0022143000015239

Schwander, J., Stauffer, B., & Sigg, A. (1988). Air mixing in firn and the age of the air at pore close-off. *Annals of Glaciology*, *10*, 141–145. https://doi.org/10.3189/S0260305500004328